Quarterly Report

Fundamental Understanding of Methane-Carbon Dioxide-Water (CH$_4$-CO$_2$-H$_2$O) Interactions in Shale Nanopores under Reservoir Conditions

Oct. 27, 2015

WORK PERFORMED UNDER

Field Work Proposal 14-017608

PRINCIPAL INVESTIGATOR

Yifeng Wang

Sandia National Laboratories, 1515 Eubank SE, Mail Stop 0779, Albuquerque, NM 87123; telephone: (505)844-8271; fax: (505)844-2348; e-mail: ywang@sandia.gov

U.S. DEPARTMENT OF ENERGY

Sandia National Laboratories

1.0   GOALS OF PROJECT

Shale is characterized by the predominant presence of nanometer-scale (1-100 nm) pores. The behavior of fluids in those pores directly controls shale gas storage and release in shale matrix and ultimately the wellbore production in unconventional reservoirs. Recently, it has been recognized that a fluid confined in nanopores can behave dramatically differently from the corresponding bulk phase due to nanopore confinement (Wang, 2014). CO_2 and H_2O, either preexisting or introduced, are two major components that coexist with shale gas (predominately CH_4) during hydrofracturing and gas extraction. Note that liquid or supercritical CO_2 has been suggested as an alternative fluid for subsurface fracturing such that CO_2 enhanced gas recovery can also serve as a CO_2 sequestration process. Limited data indicate that CO_2 may preferentially adsorb in nanopores (particularly those in kerogen) and therefore displace CH_4 in shale. Similarly, the presence of water moisture seems able to displace or trap CH_4 in shale matrix. Therefore, fundamental understanding of CH_4-CO_2-H_2O behavior and their interactions in shale nanopores is of great importance for gas production and the related CO_2 sequestration. This project focuses on the systematic study of CH_4-CO_2-H_2O interactions in shale nanopores under high-pressure and high temperature reservoir conditions. The proposed work will help to develop new stimulation strategies to enable efficient resource recovery from fewer and less environmentally impactful wells**.**

2.0   ACCOMPLISHMENTS

Experimental Work

<u>Acquisition of additional shale core samples:</u> We have purchased two more shale core samples: 2 kg of Marcellus sample and 2 kg of Woodford sample. Part of the samples will be sent out for isolation of kerogen. These materials, together with previously purchased Mancos shale, will be used in CH_4-CO_2-H_2O sorption/desorption measurements.

<u>Estimation of gas sorption for high pressure and high temperature experiments:</u> A typical sorption curve for a high temperature and pressure measurement is shown in Figure 1. The decrease in pressure is interpreted as absorption to adsorbent materials. The amounts of absorbed are calculated based in the differential pressure according to the compressibility factor of CH_4+CO_2 mixtures at the experimental temperature:

$$Z = \frac{(\Delta P) \times V}{n_{sorbed} \times R \times T} \tag{1}$$

where Z is the compressibility factor, V the volume of the experimental system, ΔP the difference between the initial pressure and the final pressure, T the experimental temperature, R ideal gas constant, and n_{sorbed} the moles of CH_4+CO_2 mixtures sorbed onto the model substance. In the experimental system, V and T are constant. Z is thus only a function of pressure. Rearranging Eq. (1), we have,

$$n_{sorbed} = \frac{(\Delta P) \times V}{Z \times R \times T} \tag{2}$$

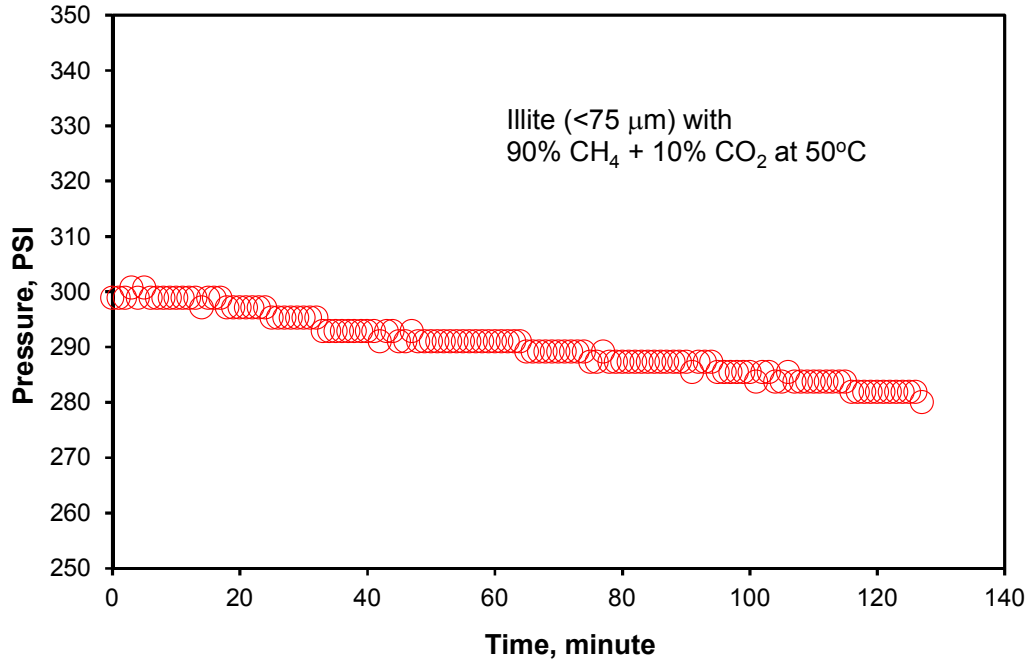Therefore, once Z at the pressure of ΔP is known, n_{sorbed} can be solved using Eq. (2).

Figure 1. Sorption of $CH_4 + CO_2$ onto illite at $50^{\circ}C$ temperature and 300 psi

McElroy et al. (1989) measured the compressibility factors for CH_4+CO_2 mixtures at CH_4 percentages of 0, 25, 75 and 100 in the temperature range from $30^{\circ}C$ to $60^{\circ}C$. We used their measured compressibility factors at $50^{\circ}C$ and at pressures ranging from 120 bars to 8 bars to develop the correlations between pressures and compressibility factors. Then, the compressibility factor at ΔP is computed based on the correlation. Using Eq. (2), the amounts absorbed are calculated, and the sorption kinetics is calculated based on the time required for reaching the sorption saturation (Table 1).

Table 1. Experimental measurement of sorption capacity and sorption rate for a model substance at an elevated temperature and pressure

Model Substances	Temp, $^{\circ}C$	Gas Mixture, volume percent	Pressure, PSI	Sorption Capacity (mixture) mg/g	Sorption Rate, mg/g min^{-1}
Illite, <75 μm	50	90% CH_4 + 10% CO_2	300	190	1.5

3

Alternatively, the following algorithm can also be used for computing the amounts of CH_4+CO_2 mixtures sorbed:

$$Z_{initial} = \frac{P_{initial} \times V}{n_{total,initial} \times R \times T}$$ (3)

$$Z_{final} = \frac{P_{final} \times V}{n_{total,final} \times R \times T}$$ (4)

$$n_{sorbed} = n_{total,initial} - n_{total,final}$$ (5)

In the future, we will first measure the compressibility factors as a function of pressures at temperatures not covered by McElroy et al. (1989). We will then conduct the sorption measurements.

Modeling Work

Molecular modeling including Monte Carlo (MC) and molecular dynamics (MD) simulations were implemented to study the adsorption and transport properties of methane within a condensed kerogen phase. The simulated kerogen represents type II-D kerogen (post mature, gas formation zone), which is similar to that found in Barnett shale (Ungerer et al., 2015). The condensed kerogen consists of 24 kerogen molecules (Figure 2) and can be simulated at different temperature and pressure. At 300 K and 1 atm the density of condensed kerogen obtained from our MD simulation is 1.20±0.02 g/ml, which is slightly smaller than that obtained from experiment (1.3-1.4 g/ml) (Okiongbo et al., 2005). The pore size distribution indicates that our kerogen model has micropores ranging from 5 to 15 Å (Figure 3). This observation is in good agreement with experimental data, except that kerogen also has macropores that are not reproduced in the simulations due to the limited length scale of the simulation box. Grand Canonical Monte Carlo simulation was used to calculate the methane adsorption isotherm (Figure 4) at 300 K for our model kerogen. The results demonstrate that methane uptake in type II-D kerogen is much higher than that observed experimentally for immature kerogens such as those found in Green River shale (Zhang et al., 2012) (Figure 5).
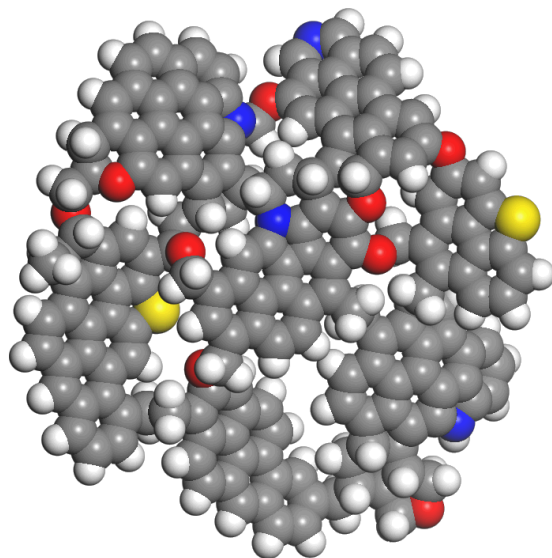
Figure 2. Snapshot illustrates kerogen molecule. Silver, white, red, blue, and yellow spheres represent carbon, hydrogen, oxygen, nitrogen, and sulfur atoms, respectively
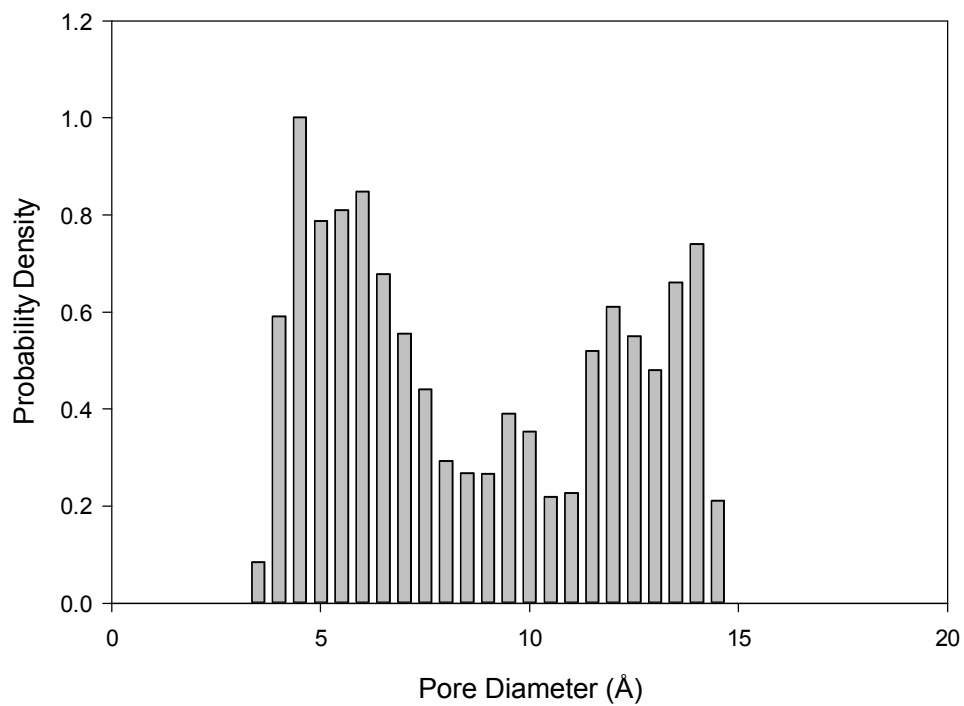

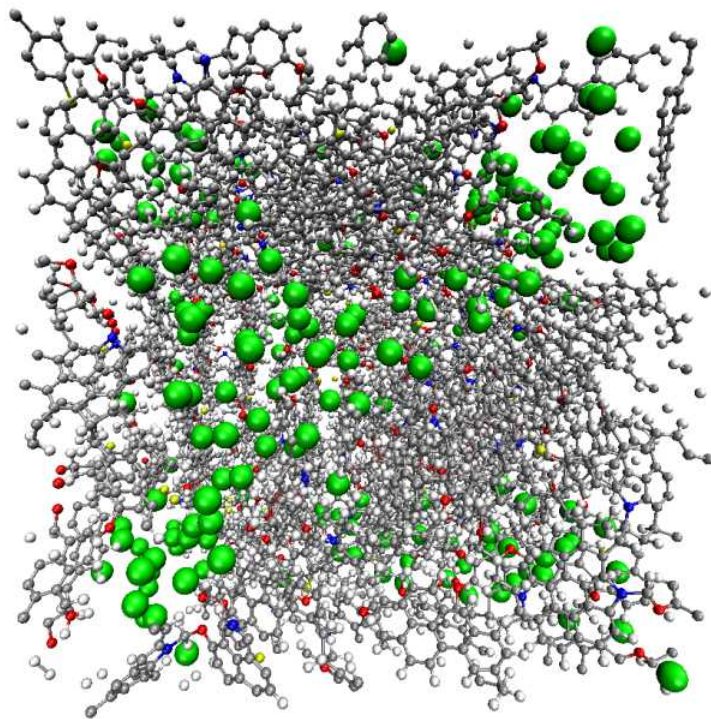**Figure 1.** Pore size distribution of condensed kerogen model

Figure 4. Representative snapshot demonstrates the adsorption of methane (green spheres) on condensed kerogen phase
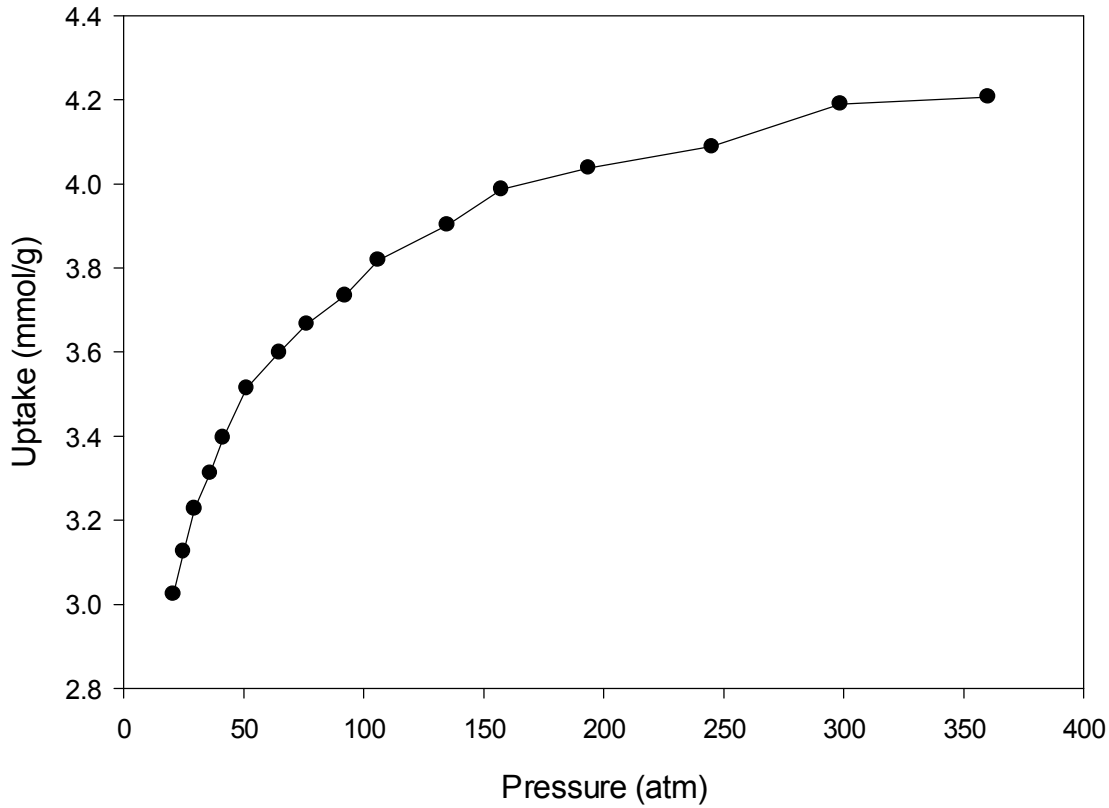
Figure 5. Methane adsorption isotherm at 300K on condensed kerogen

3.0 OUTLOOK

The next step will include:
- Expanding the low pressure sorption measurements to a full cycle of adsorption-desorption measurements. The data to be obtained will help understand the possible hysteresis behavior of gas sorption in nanopores.
- Performing high pressure and high temperature sorption measurements on crushed shale samples. Develop a highly accurate equation of state (EOS) for CH_4-CO_2 mixtures for data interpretation.
- Starting a cDFT formulation for CH_4-CO_2 sorption in nanopores and trying to apply the model to both low and high pressure measurements.

4.0 REFERENCES

McElroy, P.J., Battino, R., and Dowd, M.K. (1989) Compression-factor measurements on

methane, carbon dioxide, and (methane + carbon dioxide) using a weighing method. Journal of Chemical Thermodynamics, 21, 1287-1300.

Okiongbo, K.S., Aplin, A.C., and Larter, S.R. (2005) Changes in type II kerogen density as a function of maturity: Evidence from the Kimmeridge Clay Formation, Energy & Fuels, 19, 2495-2499.

Ungerer et al., 2015. Molecular modeling of the volumetric and thermodynamic properties of Kerogen: Influence of organic type and maturity, Energy & Fuels, 29, 91-105.

Zhang, T., Ellis, G. S., Ruppel, S.C., Milliken, K., and Yang, R. (2012) Effect of organic-matter type and thermal maturity on methane adsorption in shale gas systems, Organic Geochemistry, 47, 120-131.